

Amphipathic Side Chain of a Conjugated Polymer Optimizes Dopant Location toward Efficient N-Type Organic Thermoelectrics

Jian Liu, Gang Ye,* Hinderikus G. O. Potgieser, Marten Koopmans, Selim Sami, Mohamad Insan Nugraha, Diego Rosas Villalva, Hengda Sun, Jingjin Dong, Xuwen Yang, Xinkai Qiu, Chen Yao, Giuseppe Portale, Simone Fabiano, Thomas D. Anthopoulos, Derya Baran, Remco W. A. Havenith, Ryan C. Chiechi,* and L. Jan Anton Koster*

There is no molecular strategy for selectively increasing the Seebeck coefficient without reducing the electrical conductivity for organic thermoelectrics. Here, it is reported that the use of amphipathic side chains in an n-type donor–acceptor copolymer can selectively increase the Seebeck coefficient and thus increase the power factor by a factor of ≈ 5 . The amphipathic side chain contains an alkyl chain segment as a spacer between the polymer backbone and an ethylene glycol type chain segment. The use of this alkyl spacer does not only reduce the energetic disorder in the conjugated polymer film but can also properly control the dopant sites away from the backbone, which minimizes the adverse influence of counterions. As confirmed by kinetic Monte Carlo simulations with the host–dopant distance as the only variable, a reduced Coulombic interaction resulting from a larger host–dopant distance contributes to a higher Seebeck coefficient for a given electrical conductivity. Finally, an optimized power factor of $18 \mu\text{W m}^{-1} \text{K}^{-2}$ is achieved in the doped polymer film. This work provides a facile molecular strategy for selectively improving the Seebeck coefficient and opens up a new route for optimizing the dopant location toward realizing better n-type polymeric thermoelectrics.


polymers have also emerged as potential candidates for organic thermoelectrics,^[7,8] potentially delivering flexible, large-area, and low-cost energy generation or heating-cooling devices for appealing applications, e.g., wearable energy harvesting, that are currently not possible for traditional brittle and usually either toxic or rare inorganic crystalline thermoelectric materials. Thermoelectric materials are evaluated by the dimensionless figure of merit $ZT = S^2\sigma T/\kappa$, where S , σ , T and κ represent the Seebeck coefficient, electrical conductivity, absolute temperature and thermal conductivity, respectively. Most conjugated polymers are characterized with low κ values, intrinsically contributing to a high ZT . This point has been verified by recent extensive thermoelectric studies based on p-type conjugated polymers such as poly(3,4-ethylenedioxythiophene) (PEDOT) with $ZT > 0.25$.^[9,10] The performance of p-type and n-type thermoelectric materials should pair with each other ahead of any practical applications. However, n-type conjugated polymer-based thermoelectric devices are still far inferior to their p-type counterparts in terms of power factor ($S^2\sigma$).^[11,12] Therefore, the development of efficient

Conjugated polymers have been successfully exploited in a wide range of applications including optoelectronic devices, electrochemical energy storage, and sensors because of their natural advantages, such as low material cost, mechanical flexibility, low toxicity, and lightweight.^[1–6] Recently, conjugated

manance of p-type and n-type thermoelectric materials should pair with each other ahead of any practical applications. However, n-type conjugated polymer-based thermoelectric devices are still far inferior to their p-type counterparts in terms of power factor ($S^2\sigma$).^[11,12] Therefore, the development of efficient

Dr. J. Liu, Dr. G. Ye, H. G. O. Potgieser, M. Koopmans, S. Sami, J. Dong, X. Yang, X. Qiu, Dr. G. Portale, Dr. R. W. A. Havenith, Prof. R. C. Chiechi, Prof. L. J. A. Koster
Zernike Institute for Advanced Materials
University of Groningen
Nijenborgh 4, Groningen NL-9747 AG, the Netherlands
E-mail: g.ye@rug.nl; r.c.chiechi@rug.nl; l.j.a.koster@rug.nl
Dr. G. Ye, S. Sami, X. Qiu, C. Yao, Dr. R. W. A. Havenith, Prof. R. C. Chiechi
Stratingh Institute for Chemistry
University of Groningen
Nijenborgh 4, Groningen NL-9747 AG, The Netherlands

Dr. M. I. Nugraha, D. R. Villalva, Prof. T. D. Anthopoulos, Prof. D. Baran
King Abdullah University of Science and Technology (KAUST)
Physical Science and Engineering Division (PSE)
KAUST Solar Center (KSC)
Thuwal 23955-6900, Saudi Arabia
Dr. H. Sun, Dr. S. Fabiano
Laboratory of Organic Electronics
Department of Science and Technology
Linköping University
Norrköping SE-601 74, Sweden
Dr. R. W. A. Havenith
Department of Inorganic and Physical Chemistry
Ghent University
Krijgslaan 281-(S3), Ghent B-9000, Belgium

 The ORCID identification number(s) for the author(s) of this article can be found under <https://doi.org/10.1002/adma.202006694>.

© 2020 The Authors. Advanced Materials published by Wiley-VCH GmbH. This is an open access article under the terms of the Creative Commons Attribution-NonCommercial-NoDerivs License, which permits use and distribution in any medium, provided the original work is properly cited, the use is non-commercial and no modifications or adaptations are made.

DOI: 10.1002/adma.202006694

n-type polymer thermoelectrics deserves and requires more attention from the community.

One key parameter for optimizing power factors is the electrical conductivity, which is defined by $\sigma = q \times \mu \times n$ (where μ and n are the mobility and free carrier density, respectively). The carrier density is modulated by molecular doping, which often involves a redox reaction with a strong reducing agent (n-type dopant).^[13–17] As such, the quest for n-type conjugated polymers with high electron mobility and large electron affinity has become an obvious way to advance n-type polymeric thermoelectrics. Fortunately, molecular strategies for tuning transport properties and energetics have been extensively investigated in other research fields such as organic field-effect transistors and organic photovoltaics,^[18,19] and abundant experience has been accumulated. Benefitting from this, various backbone structures of n-type conjugated polymers with meticulous designs, such as halogen substitution,^[20,21] embedding sp^2 -N,^[22,23] incorporating novel block units,^[24] and conformation lock,^[25] have been reported to increase electrical conductivity. As is well known, there is a tradeoff between σ and S when optimizing the power factor by modulating the doping level,^[26] and it is poorly understood what determines the magnitude of the Seebeck coefficient. Most previous strategies for increasing electrical conductivity are usually at a cost of reducing the Seebeck coefficient. Moreover, there is a lack of molecular strategy for selectively increasing the Seebeck coefficient without reducing the electrical conductivity.

How impurity dopants are located within inorganic crystal lattices (interstitial or substituted) often plays a critical role in the doping process, sometimes even reversing the polarity of doped materials.^[27] However, this aspect of research has been rarely carried out in the doping of organic semiconductors probably due to the involvement of a complex doping process, intrinsic structural and energetic disorder, and large dopant size. Recently, Thomas et al. revealed that branched side chains of polythiophenes govern the dopant position within π -faces of crystallites, impacting the electrical conductivity by two orders of magnitude.^[28] Moreover, it was reported that polar ethylene glycol type side chains for conjugated polymers can effectively confine dopant molecules, leading to a negligible effect on the π - π packing and increased doping efficiency and electrical conductivity.^[29–32] These studies clearly suggest enormous potential for better control over how dopants are incorporated into a host matrix to improve thermoelectric performance.

In this work, we report that by using amphipathic side chains for a donor–acceptor (D–A) copolymer we are able to selectively increase the Seebeck coefficient, and, thus, the power factor by a factor of ≈ 5 . Distinct from previously reported conjugated copolymers with merely either alkyl side chains or ethylene glycol type side chains on acceptor moieties,^[11,21,30] herein, the conjugated copolymer with amphipathic side chains contains an alkyl chain segment as a spacer between the backbone and ethylene glycol type chain segment. The use of this alkyl spacer can not only reduce the energetic disorder of the conjugated polymer film but also properly control the dopant sites away from the backbone as evidenced by atomistic molecular dynamics (MD) simulations. The large backbone-dopant distance helps minimizing the adverse influence of counterions. As confirmed by kinetic Monte Carlo simulations with the

host-dopant distance as the only variable, the reduced Coulombic interaction resulting from a larger host-dopant distance contributes to a higher Seebeck coefficient for a given electrical conductivity. This study provides a facile molecular strategy for selectively improving the Seebeck coefficient and opens up a new route for optimizing the doping process for advancing n-type organic thermoelectrics.

Figure 1A shows chemical structures of two D–A conjugated copolymers (PNDI2TEG-2Tz and PNDI2C8TEG-2Tz) together with the dopant (4-(1,3-dimethyl-2,3-dihydro-1H-benzimidazol-2-yl)phenyl) dimethylamine (n-DMBI). Both D–A copolymers use a naphthalene(NDI)-*alt*-bithiazole (2Tz) based backbone. A NDI-2Tz backbone functionalized with linear ethylene glycol type side chains (PNDI2TEG-2Tz) was recently demonstrated as a good host for n-type polymeric thermoelectrics.^[22] The glycol type side chains were found to improve the host/dopant miscibility, and, thus, the doping efficiency.^[30] However, the substitution of alkyl by a glycol chain on the backbone leads to adverse effects on the π - π stacking, and, thus, decreases the charge mobility,^[30,33,34] which compromises the thermoelectric performance.

With the above insights in mind, we designed a novel NDI-2Tz-based copolymer (PNDI2C8TEG-2Tz) with amphipathic side chains on acceptor moieties. In PNDI2C8TEG-2Tz, an alkyl chain segment exists between the backbone and glycol chain segment. By using the amphipathic side chains, we aimed to mitigate the negative effects of glycol type side chains on the backbone stacking. It has been well established by previous experimental and simulation work that polar dopant molecules are more likely to reside within the phase of the glycol type chains rather than that of the alkyl chains.^[29,30,35] Inspired by this important point, we attempt to control the spatial location of dopants relative to the backbone by tailoring the side chains as illustrated in Figure 1B. The additional alkyl chain segment spacer is supposed to increase the backbone-dopant distance in doped PNDI2C8TEG-2Tz, compared to that in doped PNDI2TEG-2Tz. This point will be discussed in the next sections.

Both PNDI2TEG-2Tz and PNDI2C8TEG-2Tz copolymers were synthesized through a copper iodide (CuI)-assisted Pd-catalyzed Stille coupling polycondensation reaction between brominated NDI monomer (NDI2TEG or NDI2C8TEG) and stannylated bithiazole monomer (2Tz) derivatives and then fully characterized (see Schemes S1–S2 and Figures S1–S2 in the Supporting Information). Both conjugated copolymers show excellent thermal stability with a decomposition temperature (5% weight loss) of over 320 °C, as determined by thermogravimetric analysis (TGA), with no distinct phase transition observed in the range from room temperature to 300 °C by differential scanning calorimetry (DSC) (Figure S3, Supporting Information). Cyclic voltammetry characterization for the two copolymers (PNDI2TEG-2Tz and PNDI2C8TEG-2Tz) was carried out to investigate the effects of side chain modification on the energy levels (see Figure S4 in the Supporting Information). The introduction of an alkyl chain spacer between the backbone and polar glycol side chain was found to have negligible influence on the lowest unoccupied molecular orbital (LUMO) (−4.29 eV for PNDI2TEG-2Tz and −4.26 eV PNDI2C8TEG-2Tz) and the highest occupied molecular orbital (HOMO) (−5.48 eV

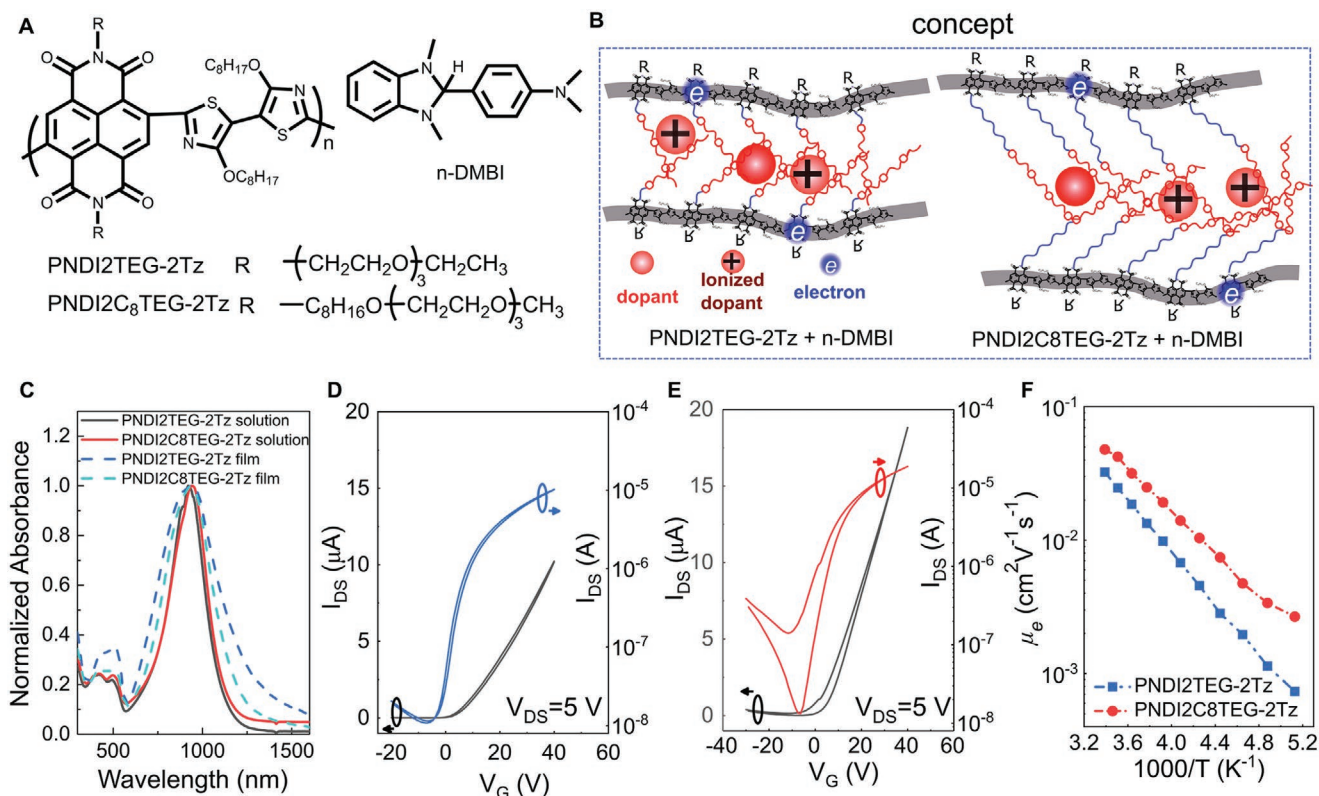


Figure 1. A) The chemical structures for PNDI2TEG-2Tz, PNDI2C8TEG-2Tz, and n-DMBI. B) An illustration of the concept of controlling the dopant position relative to the backbone by tailoring side chains. C) the UV–VIS–NIR absorption spectra of pristine PNDI2TEG-2Tz and PNDI2C8TEG-2Tz in chloroform solution and solid film. D,E) Top-gate/bottom-contact OTFT transfer characteristics of PNDI2TEG-2Tz and PNDI2C8TEG-2Tz based devices. F) The temperature dependent electron mobilities of the two conjugated copolymers.

for PNDI2TEG-2Tz and -5.49 eV PNDI2C8TEG-2Tz) levels (Table S1, Supporting Information).

Figure 1C displays the normalized UV–Vis–NIR absorption spectra measured for pristine PNDI2TEG-2Tz and PNDI2C8TEG-2Tz in chloroform solution and the thin-film state. Three neutral peaks were observed at 438, 510, and 940 nm for the various samples. We assigned the first two peaks to the π – π^* transition and the third peak to the characteristic intramolecular charge transfer.^[36] We barely observe any obvious redshifts for the peaks from the solution to the solid state, indicating very good backbone planarity for the two copolymers. Interestingly, the two copolymers exhibit nearly identical absorption spectra in solution while exhibiting very distinct features in a thin film in terms of the π – π^* transition intensity relative to the intramolecular charge-transfer transition and band-tail absorption. The higher volume fraction of the ethylene glycol type chains increases the polarizability around the PNDI2TEG-2Tz backbone. This can be considered as the solid-state equivalent of solvatochromism, which affects the charge-transfer band, and, thus, the absorption spectra for the thin-film state.

We investigated the charge transport properties of pristine PNDI2TEG-2Tz and PNDI2C8TEG-2Tz films by using bottom contact/top gate field-effect transistors (see details in Figure S5 in the Supporting Information). The electron mobility for PNDI2TEG-2Tz and PNDI2C8TEG-2Tz was determined to be 0.035 and $0.048 \text{ cm}^2 \text{V}^{-1} \text{s}^{-1}$, respectively, at room

temperature (Figure 1D,E). Figure 1F displays the Arrhenius plots for the mobility as a function of temperature, from which the activation energy for PNDI2TEG-2Tz and PNDI2C8TEG-2Tz was determined to be 196 and 154 meV, respectively. The small activation energy for the latter copolymer indicates reduced energetic disorder and traps compared to the former. This likely originates from improved molecular stacking or mitigated electronic coupling between the backbone and the glycol chains after substitution of the glycol chains for the amphipathic side chains. The thermal expansion behaviors for the two copolymer films was measured by dynamic ellipsometry (Figure S6 in the Supporting Information). We extracted a linear thermal expansion coefficient of 7.1×10^{-3} and $5.7 \times 10^{-3} \text{ K}^{-1}$ for PNDI2TEG-2Tz and PNDI2C8TEG-2Tz, respectively. The longer side chains of the latter increases the volume ratio of the soft phase over the rigid backbone, which should enhance the film expansion; the opposite trend suggests a closer chain packing for PNDI2C8TEG-2Tz compared to the other polymer.

To investigate the effects of the side chain variation and molecular doping on the molecular packing, we carried out 2D grazing incidence wide angle X-ray scattering (GIWAXS) measurements for the pristine and doped conjugated copolymers (Figure S7, Supporting Information). The PNDI2TEG-2Tz chain tends to pack mostly with an edge-on orientation relative to the substrate. As shown in Figure S7c,d (Supporting Information), the (100) and (200) peaks at $q_z = 0.26 \text{ \AA}^{-1}$ and 0.53 \AA^{-1} and two (010) peaks at $q_{xy} = 1.4 \text{ \AA}^{-1}$ and 1.75 \AA^{-1} were clearly observed for

the pristine film. This indicates a lamellar packing with characteristic interlayer distance of 2.35 nm along the out-of-plane q_z direction and π - π stacking distances of 0.40 and 0.36 nm. The (010) peak at $q_{xy} = 1.75 \text{ \AA}^{-1}$ likely originates from the π - π stacking of thiazole moiety.^[37] Upon doping, the dopant might be incorporated into the side chain phase of the PNDI2TEG-2Tz as the lamellar stacking distance is increased to 2.43 nm with the π - π stacking distance remaining the same. Additionally, the film crystallinity of the PNDI2TEG-2Tz was slightly reduced upon n-doping. Distinct from the PNDI2TEG-2Tz, the PNDI2C8TEG-2Tz chain appears to adopt a bimodal orientation with both edge-on and face-on fractions: a (100) peak at $q_{xy} = 0.19 \text{ \AA}^{-1}$ and a (010) peak at $q_z = 1.75 \text{ \AA}^{-1}$ were observed together with a (100) peak at $q_z = 0.19 \text{ \AA}^{-1}$ and (010) peaks at $q_{xy} = 1.4 \text{ \AA}^{-1}$ and 1.75 \AA^{-1} . As such, the lamellar stacking distance of the PNDI2C8TEG-2Tz film is determined to be ≈ 3.25 nm, which is larger than that (2.35 nm) of the PNDI2TEG-2Tz film. The larger spacing of lamellar stacking is expected to provide more free space to better accommodate dopant molecules. Additionally, the bimodal orientation has been reported to be beneficial for bulk charge transport and for host/dopant miscibility.^[21,38,39] Very interestingly, upon doping, the crystallinity of the edge-on lamellar domains in the PNDI2C8TEG-2Tz was apparently enhanced, which is beneficial for the in-plane charge transport.

Molecular packing and preferred dopant sites were resolved by atomistic molecular dynamics (MD) simulations for both molecules with force fields generated using the Q-Force methodology.^[40,41] Based on the 2D-GIWAXS data, a bias was imposed to preserve the lamellar packing, while dopant positions, side chain arrangements and the π - π stacking distances were relaxed. For each molecule, about 480 unique realizations of the morphology were generated, which contained 6 monomer units per n-DMBI, of which 50% was positively charged. Further computational details can be found in the Supporting Information. Representative morphologies from the MD simulations can be seen in **Figure 2A,B** for PNDI2TEG-2Tz and PNDI2C8TEG-2Tz, respectively. Several attributes of the molecular packing shown here are shared between most realizations, such as the formation of highly ordered π - π stacking layers, positioning of the dopant in between two backbone layers, and a larger lamellar spacing for PNDI2C8TEG-2Tz.

A deeper insight on π - π stacking and dopant positioning can be obtained by a statistical analysis of the morphologies. The π - π stacking distance is computed to be ≈ 0.35 nm (Figure S8, Supporting Information), in agreement with the GIWAXS measurements. No significant difference is observed between the two molecules in terms of the π - π stacking distance. The radial distribution functions (RDFs) between dopants (neutral and cationic) and the backbone of the polymers (Figure 2C), ethylene glycol side chain units (Figure 2D), and alkyl side chain units (Figure 2E) were computed in order to investigate the arrangement of the dopants within the lamellar structure. Backbone-dopant RDFs show that there is a significantly higher amount of such pairs in the short range (0.4–1.5 nm) for PNDI2TEG-2Tz, indicating a larger separation between the dopant and backbone for PNDI2C8TEG-2Tz. The separation is less for the uncharged n-DMBI, but the difference is not significant. Ethylene glycol-dopant RDFs clearly indicate that there

is a strong preference for the dopant being surrounded by ethylene glycols (0.4–1.0 nm). This effect is strongest between PNDI2C8TEG-2Tz and n-DMBI(+), followed by the PNDI2TEG-2Tz and n-DMBI(+) pair, indicating that the cationic n-DMBI has a stronger preference to be surrounded by ethylene glycols than the neutral one. Similar observations can be made from the alkyl-dopant RDFs; alkyl chains have a much less preference for being the first neighbor of n-DMBI(+) due to its strong preference for ethylene glycols. The MD simulation results validate the proposed concept that the amphipathic side chains could govern the dopant position away from the backbone, as compared to the polar side chains.

Both conjugated copolymers exhibit fibril-textured morphologies, and the domains within the PNDI2C8TEG-2Tz film appear to pack more closely together compared to the other polymer film, as evidenced by atomic force microscopy (AFM) characterization (Figure S9 in the Supporting Information). Upon mixing with the dopant, only a few aggregates were observed on the surfaces of both copolymers at higher doping concentrations, indicating good host/dopant miscibility. For PNDI2C8TEG-2Tz, this was likely enabled by the polar side chain segments, large lamellar stacking distance, or bimodal orientation, and may guarantee efficient n-doping. We examined the morphology stabilities of the pristine and doped copolymer films stored in ambient for various periods by using optical microscopy (see the results in Figure S10 in the Supporting Information). It appears that these samples are stable with minor changes after storage in ambient for 27 d.

n-DMBI has been proven to be effective to n-dope various n-type conjugated polymers,^[21,22] and shows good miscibility with the two D-A copolymers presented in this study. **Figure 3** displays the thermoelectric parameters (electrical conductivity, Seebeck coefficient and power factor) as a function of n-DMBI loading for both copolymer thin films (see details in Figures S11–S12 in the Supporting Information). The doped PNDI2TEG-2Tz film exhibits an optimized electrical conductivity of 1.36 S cm^{-1} at a dopant loading of 7 wt%. A slightly higher value of $1.6 \pm 0.1 \text{ S cm}^{-1}$ was obtained for doped PNDI2C8TEG-2Tz at a doping concentration of 5 wt%. Although the two copolymers render comparable electrical conductivities upon doping, the Seebeck coefficients for the two doped polymers are distinctly different: the copolymer with amphipathic side chains shows a much larger absolute value than the other copolymer with glycol type side chains at each doping concentration. At the maximum conductivity, the doped PNDI2C8TEG-2Tz film displays a Seebeck coefficient of $-326 \pm 31 \text{ \mu V K}^{-1}$, which is nearly double that of the doped PNDI2TEG-2Tz film ($-167 \pm 13 \text{ \mu V K}^{-1}$). The doped PNDI2TEG-2Tz film exhibits an optimized power factor of $3.8 \pm 0.6 \text{ \mu W m}^{-1} \text{ K}^{-2}$, which is consistent with our previous report.^[22] Notably, a much higher power factor of $16.5 \pm 1.2 \text{ \mu W m}^{-1} \text{ K}^{-2}$ was achieved for the doped PNDI2C8TEG-2Tz film. This result is the best value ever reported among all NDI-based conjugated polymers (Table S2, Supporting Information).

As PNDI2C8TEG-2Tz has longer side chains on the NDI moiety than PNDI2TEG-2Tz, one may ask whether or not the different lengths of the side chain lead to the distinct thermoelectric performance. To answer this question, we synthesized a new conjugated polymer PNDI2HexEG-2Tz (see

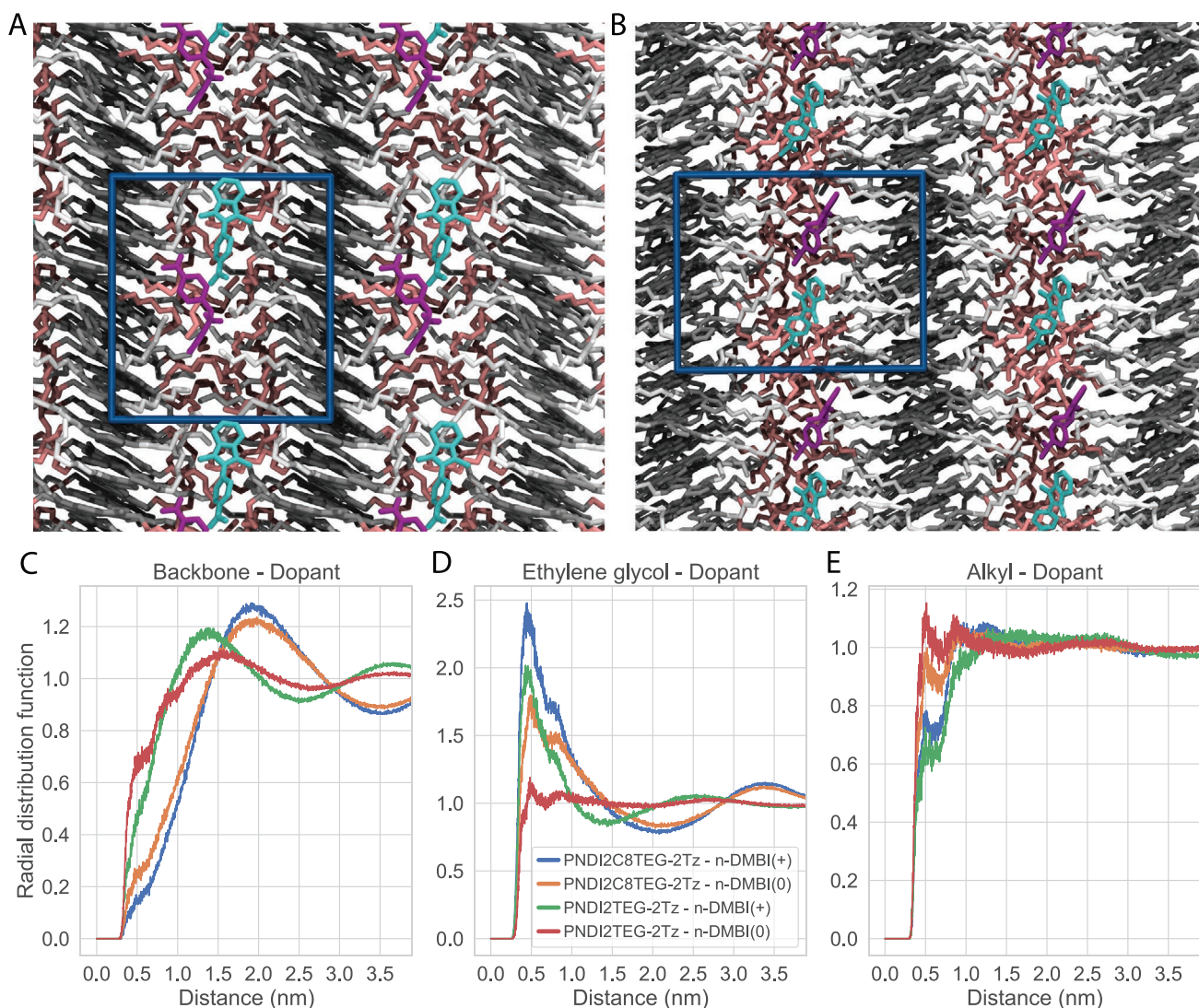


Figure 2. Representative morphologies from the MD simulations for A) PNDI2TEG-2Tz and B) PNDI2C8TEG-2Tz. Dark gray = backbone, white = alkyl units, light red = ethylene glycol units, green = n-DMBI(+), purple = n-DMBI(0). Radial distribution functions (RDFs) between n-DMBI (both cationic and neutral) and both C) molecule's backbone, D) ethylene glycol side chain units, and E) alkyl side chain units.

the synthetic routine in the Supporting Information), which has the polar side chain with a length similar to the amphipathic side chain of PNDI2C8TEG-2Tz. This copolymer was doped by n-DMBI with various weight percents and the thermoelectric parameters are plotted in Figure S13 (Supporting Information). As compared to PNDI2TEG-2Tz, the long polar side chains of PNDI2HexEG-2Tz appear to facilitate the molecular doping with improved electrical conductivities, reduced absolute Seebeck coefficients but comparable power factors. For example, the 5wt%-doped PNDI2HexEG-2Tz gives an electrical conductivity of 3.3 S cm^{-1} , a Seebeck coefficient of $-115 \text{ } \mu\text{V K}^{-1}$, and a power factor of $4.3 \text{ } \mu\text{W m}^{-1} \text{ K}^{-2}$. Thus we come to conclude that the selectively enhanced Seebeck coefficient observed for the doped PNDI2C8TEG-2Tz mostly results from the amphipathic side chains rather than the increased side-chain length.

The molecular doping of conjugated polymers generates polarons, which often leads to distinct absorption features in UV-Vis-NIR absorption spectra for pristine films. **Figure 4A** demonstrates how the absorption spectra for both conjugated polymer-based films change upon incorporation of an n-DMBI admixture (5 wt%). The doping of the conjugated polymers is accompanied by a redshift and quenching of low energy neutral absorption bands along with the formation of a band-tail absorption at $\approx 1300 \text{ nm}$ (P2) and a broad absorption band at wavelengths $>1800 \text{ nm}$ (P1). The larger doping-induced quenching of the intramolecular charge transfer transition peak for PNDI2TEG-2Tz indicates a relatively stronger redox reaction with the dopant compared to that within the other blend. This is also supported by the stronger polaron absorption bands (P1 and P2) observed in the doped PNDI2TEG-2Tz. Since the two copolymers have the same backbone with

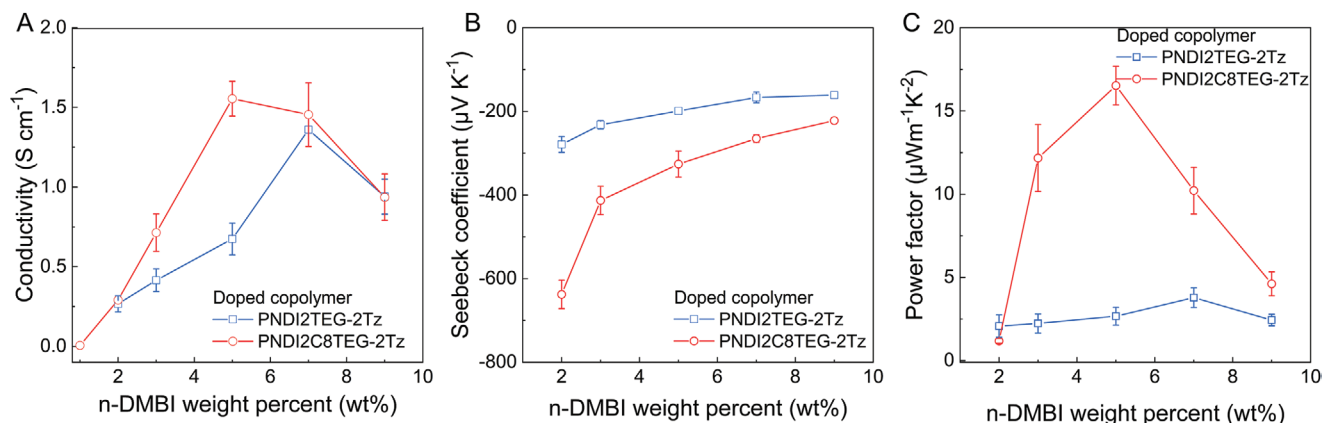


Figure 3. The A) electrical conductivity, B) Seebeck coefficient, and C) power factor of various doped PNDI2TEG-2Tz and PNDI2C8TEG-2Tz film.

identical electron affinity, the different degrees of redox reactions can be supposed to originate from the effects of the side chains. As revealed by the morphological study of the doped films, the dopant has a similar solubility in the matrix of both copolymers, which excludes the mixing quality as the determining factor for the observation of different n-doping levels. As such, the most likely factor affecting the doping levels at a molecular level is the charge/hydride transfer between the backbone and the dopant. In the doped PNDI2C8TEG-2Tz,

the dopant confined within the phase of glycol chain segments is more distant from the NDI moiety compared to the doped PNDI2TEG-2Tz (as evidenced by MD simulations in Figure 2). This may result in relatively weaker charge/hydride transfer in the doped PNDI2C8TEG-2Tz. Previous studies indicate that the energetics of the host and dopant plays an important role in the charge-transfer doping.^[20,42] The PNDI2C8TEG-2Tz has fewer band-tail states that are energetically favorable for the charge transfer as compared to PNDI2TEG-2Tz. This aspect may also

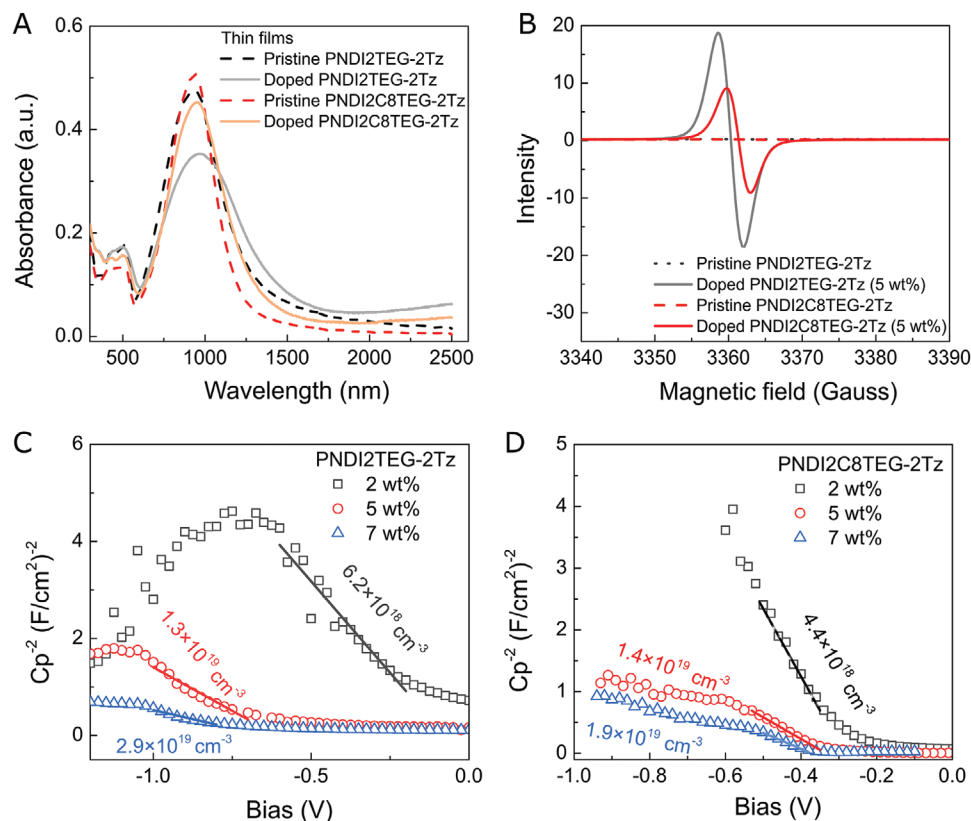


Figure 4. The characteristics of polaron and free charge generation by doping. A) the UV-VIS-NIR absorption spectra of pristine and 5 wt%-doped conjugated copolymers, and B) the corresponding EPR spectra at the same conditions; the Mott-Schottky plots of various C) doped PNDI2TEG-2Tz and D) doped PNDI2C8TEG-2Tz films. The capacitance were measured at a frequency of 10 Hz, and the extracted free-charge densities are indicated next to the corresponding curves.

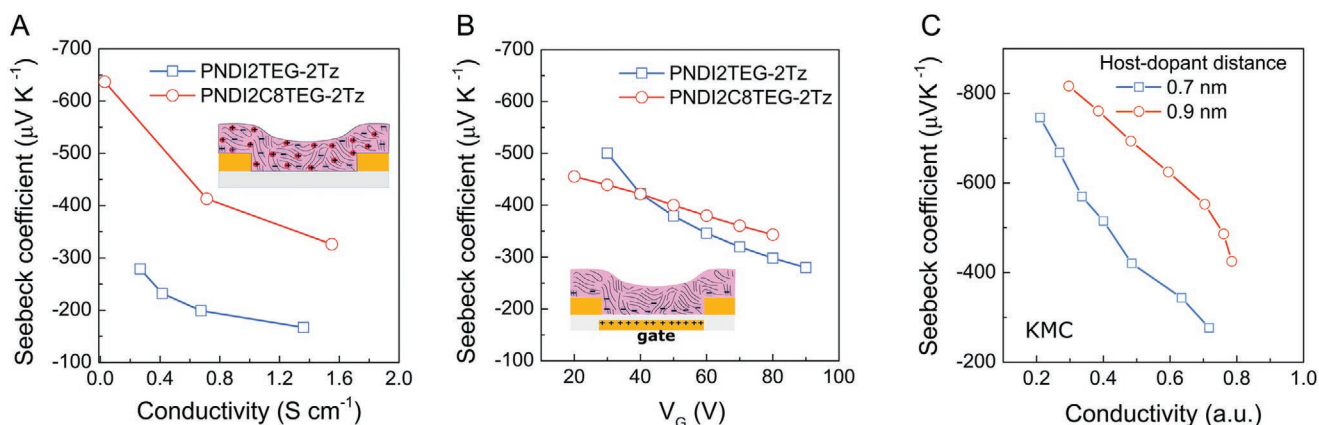


Figure 5. A) Experimental S – σ plots for molecularly doped PNDI2TEG-2Tz and PNDI2C8TEG-2Tz films. B) The field-effect Seebeck coefficients for PNDI2TEG-2Tz and PNDI2C8TEG-2Tz films, as determined using transistor devices. C) The KMC simulated S – σ relations at host-dopant distances of 0.7 and 0.9 nm.

contribute to the observation of weak charge transfer from the dopant to the host.

To further determine polaron generation upon doping, we performed electron paramagnetic resonance (EPR) measurements for pristine and doped (5 wt%) copolymer films. In the EPR spectroscopy, very weak radical signals were observed in both pristine conjugated polymers, as shown in Figure 4B, which was attributed to the characteristic intramolecular ground-state charge transfer of a typical D–A copolymer. The spin density for various polymeric films was calculated to quantitatively determine the concentration of radical species; 5 wt%-doped PNDI2TEG-2Tz exhibits a spin density of $6.4 \times 10^{19} \text{ cm}^{-3}$, while the doped PNDI2C8TEG-2Tz shows a lower spin density of $3.59 \times 10^{19} \text{ cm}^{-3}$ at the same doping condition. This indicates more polarons are generated in the former (at 5 wt% doping), which is consistent with the UV–vis–NIR absorption spectra measured for the doped films.

However, not every polaron becomes a free charge carrier that contributes to charge transport. A fraction of these polarons are localized within individual polymer chains because of a strong Coulombic interaction with counterions or large backbone distortion induced by charging.^[43,44] To extract the free charge density, we employed admittance spectroscopy for ion-gel-based metal–insulator–semiconductor (MIS) devices (see details in the Supporting Information).^[30,45] This technique is based on field-effect modulation of the depletion region in devices, which occurs in the vicinity of the contact between the ion gel dielectric layer and doped organic film, and capacitive measurement of the whole MIS device at a certain frequency. Therefore, the charged species detected by this technique are, thus, mobile (which can freely drift in to/out of the depletion region) at the used frequency compared to localized polarons. Figure 4C,D display the Mott–Schottky plots obtained for MIS devices based on doped PNDI2TEG-2Tz and PNDI2C8TEG-2Tz films at a frequency of 10 Hz. The Mott–Schottky analysis gives the free-carrier density as:^[43]

$$n = \frac{2}{q\epsilon_0\epsilon_r} \frac{\partial C_p^{-2}}{\partial V} \quad (1)$$

where ϵ_r and C_p is the dielectric constant of the active layer and the total capacitance of the MIS devices, respectively. The free carrier density in the doped PNDI2TEG-2Tz film was determined to be 6.2×10^{18} , 1.4×10^{19} , and $2.9 \times 10^{19} \text{ cm}^{-3}$ at doping concentrations of 2 wt%, 5 wt%, and 7 wt%, respectively. Similarly, doping PNDI2C8TEG-2Tz results in a carrier density of $4.4 \times 10^{18} \text{ cm}^{-3}$ at 2 wt% doping, $1.3 \times 10^{19} \text{ cm}^{-3}$ at 5 wt% doping, and $1.9 \times 10^{19} \text{ cm}^{-3}$ at 7 wt% doping. The contribution of varying free charge density to the Seebeck coefficient can be quantitatively described as $\partial S = -\frac{k_B}{q} \partial \ln(n)$ ($k_B/q = 86.3 \mu\text{V K}^{-1}$).^[46] Given that the maximum difference between the free charge densities of two doped copolymers is within a factor of 1.5, it translates into a variation in Seebeck coefficient of $\approx 35 \mu\text{V K}^{-1}$. The relatively minor contribution from the free charge density variation may not explain the large differences of their Seebeck coefficients (e.g., $-279 \mu\text{V K}^{-1}$ for 2 wt%-doped PNDI2TEG-2Tz versus $-639 \mu\text{V K}^{-1}$ for 2 wt%-doped PNDI2C8TEG-2Tz as shown in Figure 3B).

The most important finding of the present work is that the Seebeck coefficient can be increased without reducing the electrical conductivity by using amphiphathic side chains. This point is well illustrated by the experimental S – σ plots obtained for the two doped copolymers, as shown in Figure 5A: at the same electrical conductivity, the doped PNDI2C8TEG-2Tz film exhibits a much higher absolute value for the Seebeck coefficient compared to the doped PNDI2TEG-2Tz film. The doping process generates not only charges on the conjugated polymers but also counterions (the ionized dopants) for stabilizing the charges. Unlike the molecular doping method, electrical gating of a conjugated polymer film in a field-effect transistor device generates charges only within a thin polymer layer close to the dielectric layer.^[47] We carried out field-effect Seebeck coefficient measurements using a bottom contact/top gate transistor device (see Supporting Information for details), and the Seebeck coefficient–gate voltage (V_G) plots for the two D–A conjugated polymer-based devices are displayed in Figure 5B. As the field-effect mobilities for the two copolymers are very close to each other, the V_G , thus, scales with the charge carrier density and electrical conductivity of the thin copolymer layer at each gating condition. The relatively smaller dependence of the Seebeck

coefficient on the V_C for the pristine PNDI2C8TEG-2Tz might be explained by the reduced traps and disorder.^[47] It appears that the difference between the field-effect Seebeck coefficients for the two conjugated polymers is much smaller than that found for the molecular doping. This indicates that the S – σ relationship is influenced by the presence of counterions.

To better understand the effect of the host-dopant distance on the molecular doping and the thermoelectric performance from the perspective of the Coulombic interaction between the charge carrier and the counterion, we used the open-source software Excimontec to perform kinetic Monte Carlo (KMC) simulations^[48] to mimic the steady-state transport of polarons in disordered doped conjugated polymers (see details in Figure S14 in the Supporting Information). In this model, the disordered conjugated polymer was mathematically represented by a cubic lattice dimension of 70, corresponding to 70^3 lattice sites which can be occupied by charge carriers. The lattice distance was set to 1 nm, the sites were assumed to be Gaussian distributed in energy, and carrier-carrier and carrier-dopant Coulombic interactions were taken into account. The host-dopant distance was tuned by the size (r) of the dopant and every input dopant molecule was assumed to donate a charge. Figure S15 (Supporting Information) shows the simulated plots for the fraction of the total input charges located away from the dopant site as a function of the total input charges at dopant sizes of 0.7 and 0.9 nm. Otherwise, the charges sitting on the dopant sites were considered to be completely localized by the Coulombic interaction from the counterions. The simulated results indicate that a large host-dopant distance can help to reduce the charge localization by mitigating or screening the Coulombic interaction from counterions, and thus enhances the free charge generation. Previous studies have indicated that large energetic disorder can facilitate free charge generation from polarons;^[49,50] however, this is detrimental to charge mobility. In contrast, the present side chain strategy promotes the free charge generation without sacrificing the charge mobility. Figure 5C displays the simulated Seebeck coefficient as a function of the arbitrary electrical conductivity at host-dopant distances of 0.7 and 0.9 nm. At the same conductivity point, the absolute Seebeck coefficients in the two simulated systems are arranged with the order of $r = 0.9 \text{ nm} > r = 0.7 \text{ nm}$. This strongly indicates that the amphipathic side chains can help to optimize the dopant location for minimizing the Coulombic interaction, which contributes to the right-up shift of the S – σ plot as shown in Figure 5A. It should be noted that a large host-dopant distance can also reduce the chance of orbital hybridization between the charged backbone and counterion.^[51] We do not exclude the possibility that this aspect leads to an increased Seebeck coefficient.

Based on the field-effect modulated Seebeck coefficient measurement and the KMC simulation, we can conclude that, in the present study, the dopant site position relative to the adjacent host site is the main factor determining the S – σ relationship, which can be controlled by the amphipathic side chains. Additionally, we wish to point out that the amphipathic side chain strategy does not apparently influence the energy levels and carrier mobilities in the pristine polymer films, which can be easily overlooked if judged by previous experience from molecular design. However, this turns out to be very useful for

selectively increasing the Seebeck coefficient, and, thus, the power factor of n-doped conjugated polymers.

In conclusion, we report that the use of amphipathic side chains for D–A copolymer can enable one to selectively increase the Seebeck coefficient, and, thus, the power factor by a factor of ≈ 5 . The copolymer with amphipathic side chains examined herein contains an alkyl chain segment as a spacer between the polymer backbone and an ethylene glycol type chain segment. The use of this alkyl spacer chain can not only reduce the energetic disorder for better charge transport but can also enable proper control of the dopant sites away from the backbone, which minimizes the adverse influence of the counterions. As predicted by KMC simulations with the host-dopant distance as the only variable, the reduced Coulombic interaction resulting from a larger host-dopant distance contributes to a higher Seebeck coefficient at the same electrical conductivity. This study provides a facile molecular strategy for selectively improving the Seebeck coefficient and opens up a new route for optimizing the doping process towards advancing n-type organic thermoelectrics.

Supporting Information

Supporting Information is available from the Wiley Online Library or from the author.

Acknowledgements

This study was supported by a grant from STW/NWO (VIDI 13476). This study is part of the research program of the Foundation of Fundamental Research on Matter (FOM), which is part of the Netherlands Organization for Scientific Research (NWO). This is a publication by the FOM Focus Group “Next Generation Organic Photovoltaics,” participating in the Dutch Institute for Fundamental Energy Research (DIFFER). J.D. acknowledges financial support from the China Scholarship Council. The authors thank the Center for Information Technology of the University of Groningen for their support and for providing access to the Peregrine high performance computing cluster. S.F. acknowledges the support from the Swedish Research Council (2016-03979), Olle Engkvists Stiftelse (204-0256), and the Advanced Functional Materials center at LiU (2009 00971). D.B. acknowledges the support by the King Abdullah University of Science and Technology (KAUST) Office of Sponsored Research (OSR) under Award No. OSR-CRG2018-3737. S.S. and R.W.A.H. acknowledges SURFSara for giving access to the Dutch national supercomputer Cartesius. This work was sponsored by NWO Exact and Natural Sciences for the use of supercomputer facilities (2020/ENW/00852342). The authors greatly thank dr. H.P. (Hjalmar) Permentier from Interfaculty Mass Spectrometry Center, University of Groningen for MALDI-TOF measurement.

Conflict of Interest

The authors declare no conflict of interest.

Keywords

conjugated polymers, dopant location, N-type doping, organic thermoelectrics, Seebeck coefficient, solution processing

Received: October 2, 2020

Revised: November 25, 2020

Published online: December 11, 2020

- [1] O. Inganäs, *Chem. Soc. Rev.* **2010**, *39*, 2633.
- [2] M. S. AlSalhi, J. Alam, L. A. Dass, M. Raja, *Int. J. Mol. Sci.* **2011**, *12*, 2036.
- [3] J. Yang, Z. Zhao, S. Wang, Y. Guo, Y. Liu, *Chem* **2018**, *4*, 2748.
- [4] H. Siringhaus, R. J. Wilson, R. H. Friend, M. Inbasekaran, W. Wu, E. P. Woo, M. Grell, D. D. C. Bradley, *Appl. Phys. Lett.* **2000**, *77*, 406.
- [5] O. Ostroverkhova, *Chem. Rev.* **2016**, *116*, 13279.
- [6] J. Liu, S. Zeng, Z. Zhang, J. Peng, Q. Liang, *J. Phys. Chem. Lett.* **2020**, *11*, 2314.
- [7] M. Culebras, C. Gómez, A. Cantarero, *Materials* **2014**, *7*, 6701.
- [8] B. Russ, A. Glaudell, J. J. Urban, M. L. Chabynyc, R. A. Segalman, *Nat. Rev. Mater.* **2016**, *1*, 16050.
- [9] O. Bubnova, Z. U. Khan, A. Malti, S. Braun, M. Fahlman, M. Berggren, X. Crispin, *Nat. Mater.* **2011**, *10*, 429.
- [10] Z. Fan, P. Li, D. Du, J. Ouyang, *Adv. Energy Mater.* **2017**, *7*, 1602116.
- [11] Y. Sun, C. Di, W. Xu, D. Zhu, *Adv. Electron. Mater.* **2019**, *5*, 1800825.
- [12] Y. Lu, J.-Y. Wang, J. Pei, *Chem. Mater.* **2019**, *31*, 6412.
- [13] F. Li, A. Werner, M. Pfeiffer, K. Leo, X. Liu, *J. Phys. Chem. B* **2004**, *108*, 17076.
- [14] B. Lüssem, M. Riede, K. Leo, *Phys. Status Solidi* **2013**, *210*, 9.
- [15] P. Wei, J. H. Oh, G. Dong, Z. Bao, *J. Am. Chem. Soc.* **2010**, *132*, 8852.
- [16] C.-Y. Yang, Y.-F. Ding, D. Huang, J. Wang, Z.-F. Yao, C.-X. Huang, Y. Lu, H.-I. Un, F.-D. Zhuang, J.-H. Dou, C. Di, D. Zhu, J.-Y. Wang, T. Lei, J. Pei, *Nat. Commun.* **2020**, *11*, 3292.
- [17] J. Liu, B. van der Zee, R. Alessandri, S. Sami, J. Dong, M. I. Nugraha, A. J. Barker, S. Rousseva, L. Qiu, X. Qiu, N. Klasen, R. C. Chiechi, D. Baran, M. Caironi, T. D. Anthopoulos, G. Portale, R. W. A. Havenith, S. J. Marrink, J. C. Hummelen, L. J. A. Koster, *Nat. Commun.* **2020**, *11*, 5694.
- [18] J. Hou, M.-H. Park, S. Zhang, Y. Yao, L.-M. Chen, J.-H. Li, Y. Yang, *Macromolecules* **2008**, *41*, 6012.
- [19] W. Wu, Y. Liu, D. Zhu, *Chem. Soc. Rev.* **2010**, *39*, 1489.
- [20] K. Shi, F. Zhang, C.-A. Di, T.-W. Yan, Y. Zou, X. Zhou, D. Zhu, J.-Y. Wang, J. Pei, *J. Am. Chem. Soc.* **2015**, *137*, 6979.
- [21] C.-Y. Yang, W.-L. Jin, J. Wang, Y.-F. Ding, S. Nong, K. Shi, Y. Lu, Y.-Z. Dai, F.-D. Zhuang, T. Lei, C.-A. Di, D. Zhu, J.-Y. Wang, J. Pei, *Adv. Mater.* **2018**, *30*, 1802850.
- [22] J. Liu, G. Ye, B. van der Zee, J. Dong, X. Qiu, Y. Liu, G. Portale, R. C. Chiechi, L. J. A. Koster, *Adv. Mater.* **2018**, *30*, 1804290.
- [23] S. Wang, H. Sun, T. Erdmann, G. Wang, D. Fazzi, U. Lappan, Y. Puttisong, Z. Chen, M. Berggren, X. Crispin, A. Kiriy, B. Voit, T. J. Marks, S. Fabiano, A. Facchetti, *Adv. Mater.* **2018**, *30*, 1801898.
- [24] X. Yan, M. Xiong, J.-T. Li, S. Zhang, Z. Ahmad, Y. Lu, Z.-Y. Wang, Z.-F. Yao, J.-Y. Wang, X. Gu, T. Lei, *J. Am. Chem. Soc.* **2019**, *141*, 20215.
- [25] Y. Lu, Z. Yu, R. Zhang, Z. Yao, H. You, L. Jiang, H. Un, B. Dong, M. Xiong, J. Wang, J. Pei, *Angew. Chem., Int. Ed.* **2019**, *58*, 11390.
- [26] H. Wang, C. Yu, *Joule* **2019**, *3*, 53.
- [27] S. M. Sze, K. K. Ng, *Physics of Semiconductor Devices*, 3rd ed., Wiley, New York **2006**.
- [28] E. M. Thomas, E. C. Davidson, R. Katsumata, R. A. Segalman, M. L. Chabynyc, *ACS Macro Lett.* **2018**, *7*, 1492.
- [29] J. Liu, L. Qiu, G. Portale, M. Koopmans, G. ten Brink, J. C. Hummelen, L. J. A. Koster, *Adv. Mater.* **2017**, *29*, 1701641.
- [30] J. Liu, L. Qiu, R. Alessandri, X. Qiu, G. Portale, J. Dong, W. Talsma, G. Ye, A. A. Sengirian, P. C. T. Souza, M. A. Loi, R. C. Chiechi, S. J. Marrink, J. C. Hummelen, L. J. A. Koster, *Adv. Mater.* **2018**, *30*, 1704630.
- [31] D. Kiefer, A. Giovannitti, H. Sun, T. Biskup, A. Hofmann, M. Koopmans, C. Cendra, S. Weber, L. J. Anton Koster, E. Olsson, J. Rivnay, S. Fabiano, I. McCulloch, C. Müller, *ACS Energy Lett.* **2018**, *3*, 278.
- [32] J. Liu, M. P. Garman, J. Dong, B. van der Zee, L. Qiu, G. Portale, J. C. Hummelen, L. J. A. Koster, *ACS Appl. Energy Mater.* **2019**, *2*, 6664.
- [33] A. Giovannitti, I. P. Maria, D. Hanifi, M. J. Donahue, D. Bryant, K. J. Barth, B. E. Makdah, A. Savva, D. Moia, M. Zetek, P. R. F. Barnes, O. G. Reid, S. Inal, G. Rumbles, G. G. Malliaras, J. Nelson, J. Rivnay, I. McCulloch, *Chem. Mater.* **2018**, *30*, 2945.
- [34] X. Chen, Z. Zhang, Z. Ding, J. Liu, L. Wang, *Angew. Chem., Int. Ed.* **2016**, *55*, 10376.
- [35] J. Li, C. W. Rochester, I. E. Jacobs, E. W. Aasen, S. Friedrich, P. Stroeve, A. J. Moulé, *Org. Electron.* **2016**, *33*, 23.
- [36] B. D. Naab, X. Gu, T. Kurosawa, J. W. F. To, A. Salleo, Z. Bao, *Adv. Electron. Mater.* **2016**, *2*, 1600004.
- [37] Y. Shi, H. Guo, M. Qin, J. Zhao, Y. Wang, H. Wang, Y. Wang, A. Facchetti, X. Lu, X. Guo, *Adv. Mater.* **2018**, *30*, 1705745.
- [38] J. Mei, D. H. Kim, A. L. Ayzner, M. F. Toney, Z. Bao, *J. Am. Chem. Soc.* **2011**, *133*, 20130.
- [39] Y. Wang, K. Takimiya, *Adv. Mater.* **2020**, *32*, 2002060.
- [40] S. Sami, R. Alessandri, R. Broer, R. W. A. Havenith, *ACS Appl. Mater. Interfaces* **2020**, *12*, 17783.
- [41] S. Sami, M. F. S. J. Menger, S. Faraj, R. Broer, R. W. A. Havenith, *Quantum Mechanically Augmented Molecular Force Fields*, **2020**, <https://github.com/selimsami/qforce>.
- [42] X. Qiu, B. Cao, S. Yuan, X. Chen, Z. Qiu, Y. Jiang, Q. Ye, H. Wang, H. Zeng, J. Liu, M. G. Kanatzidis, *Sol. Energy Mater. Sol. Cells* **2017**, *159*, 1.
- [43] J. Liu, Y. Shi, J. Dong, M. I. Nugraha, X. Qiu, M. Su, R. C. Chiechi, D. Baran, G. Portale, X. Guo, L. J. A. Koster, *ACS Energy Lett* **2019**, *4*, 1556.
- [44] S. Wang, H. Sun, U. Ail, M. Vagin, P. O. Å. Persson, J. W. Andreasen, W. Thiel, M. Berggren, X. Crispin, D. Fazzi, S. Fabiano, *Adv. Mater.* **2016**, *28*, 10764.
- [45] J. Liu, S. Maity, N. Roosloot, X. Qiu, L. Qiu, R. C. Chiechi, J. C. Hummelen, E. Hauff, L. J. A. Koster, *Adv. Electron. Mater.* **2019**, *5*, 1800959.
- [46] K. Broch, D. Venkateshvaran, V. Lemaury, Y. Olivier, D. Beljonne, M. Zelazny, I. Nasrallah, D. J. Harkin, M. Stutz, R. Di Pietro, A. J. Kronemeijer, H. Siringhaus, *Adv. Electron. Mater.* **2017**, *3*, 1700225.
- [47] D. Venkateshvaran, M. Nikolka, A. Sadhanala, V. Lemaury, M. Zelazny, M. Kepa, M. Hurhangee, A. J. Kronemeijer, V. Pecunia, I. Nasrallah, I. Romanov, K. Broch, I. McCulloch, D. Emin, Y. Olivier, J. Cornil, D. Beljonne, H. Siringhaus, *Nature* **2014**, *515*, 384.
- [48] M. C. Heiber, *J. Open Source Software* **2020**, *5*, 2307.
- [49] M. L. Tietze, J. Benduhn, P. Pahner, B. Nell, M. Schwarze, H. Kleemann, M. Krammer, K. Zojer, K. Vandewal, K. Leo, *Nat. Commun.* **2018**, *9*, 1182.
- [50] A. Fedaii, F. Symalla, P. Friederich, W. Wenzel, *Nat. Commun.* **2019**, *10*, 4547.
- [51] I. Salzmann, G. Heimel, M. Oehzelt, S. Winkler, N. Koch, *Acc. Chem. Res.* **2016**, *49*, 370.